Syst. Biol. 74(6):935–951, 2025

https://doi.org/10.1093/sysbio/syaf033
Advance Access publication May 13, 2025

Introgression across Narrow Contact Zones Shapes the Genomic Landscape of Phylogenetic Variation in an African Bird Clade

Loïs Rancilhac[1,*], Stacey G. de Souza[1], Sifiso M. Lukhele[1], Matteo Sebastianelli[1], Bridget O. Ogolowa[1], Michaella Moysi[1], Christos Nikiforou[1], Tsyon Asfaw[2,3], Colleen T. Downs[4], Alan Brelsford[5], Bridgett M. vonHoldt[6], and Alexander N. G. Kirschel[1,*]

[1]*Department of Biological Sciences, University of Cyprus, PO Box 20537, Nicosia 1678, Cyprus*
[2]*Department of Wildlife and Protected Area Management, Wondo Genet College of Forestry and Natural Resources, Hawassa University, Wondo Genet 251 46, Ethiopia*
[3]*Evolutionary Ecology Group, Biology, University of Antwerp, Universiteitsplein 1, 2610 Wilrijk, Antwerp, Belgium*
[4]*Centre for Functional Biodiversity, School of Life Sciences, University of KwaZulu-Natal, King Edward Ave, Pietermaritzburg 3209, South Africa*
[5]*Department of Evolution, Ecology and Organismal Biology, University of California, Riverside, 900 University Ave., Riverside, CA 92521, USA*
[6]*Department of Ecology and Evolutionary Biology, 106A Guyot Hall, Princeton University, Princeton, NJ 08544, USA*
[*]*Correspondence to be sent to: Department of Biological Sciences, University of Cyprus, PO Box 20537, Nicosia 1678, Cyprus; E-mail: loisrancilhac@gmail.com; kirschel.alexander@ucy.ac.cy*

Received 29 July 2024; reviews returned 11 April 2025; accepted 5 May 2025
Associate Editor: Isaac Overcast

Abstract.—Genomic analyses of hybrid zones provide excellent opportunities to investigate the consequences of introgression in nature. In combination with phylogenomics analyses, hybrid zone studies may illuminate the role of ancient and contemporary gene flow in shaping variation of phylogenetic signals across the genome, but this avenue has not been explored yet. We combined phylogenomic and geographic cline analyses in a *Pogoniulus* tinkerbird clade to determine whether contemporary introgression through hybrid zones contributes to gene-tree heterogeneity across the species ranges. We found diverse phylogenetic signals across the genome with the most common topologies supporting monophyly among taxa connected by secondary contact zones. Remarkably, these systematic conflicts were also recovered when selecting only individuals from each taxon's core range. Using analyses of derived allele sharing and "recombination aware" phylogenomics, we found that introgression shapes gene-tree heterogeneity, and the species tree most likely supports monophyletic red-fronted tinkerbirds, as recovered in previous reconstructions based on mtDNA. Furthermore, by fitting geographic clines across two secondary contact zones, we found that introgression rates were lower in genomic regions supporting the putative species tree compared with those supporting the two taxa in contact as monophyletic. This demonstrates that introgression through narrow contact zones shapes gene-tree heterogeneity even in allopatric populations. Our results show that species can withstand important amounts of introgression while maintaining their phenotypic integrity and ecological separation, raising questions regarding the genomic architecture of adaptation and barriers to gene flow. [Birds; gene-tree heterogeneity; hybrid zones; phylogenomics; recombination; speciation.]

Phylogenetic relationships vary across the genome (Degnan and Rosenberg 2009), and whole-genome sequence studies have shown that more data may not provide a clearly conclusive phylogeny (Jeffroy et al. 2006; Bravo et al. 2019). Despite extensive efforts in the context of the multispecies coalescent framework, incomplete lineage sorting (ILS) and introgression may result in topological discordance across the genome, and thus remain a major challenge in the reconstruction of species trees (Scornavacca and Galtier 2017). Phylogenetic reconstructions are further complicated by genome-wide heterogeneity in recombination rate, selection, and demographic events (Pease and Hahn 2013; Schumer et al. 2018; Li et al. 2019; Musher et al. 2024; Thom et al. 2024). Although reconstructing the species tree remains a core goal of phylogenetics, studying patterns of gene-tree heterogeneity can illuminate the genetic architecture of reproductive barriers (Stankowski et al. 2024), and reveal the processes underlying repeated evolution of phenotypic traits (Alaei Kakhki et al. 2023; Rancilhac et al. 2024). Investigating gene-tree heterogeneity can thus yield insights into the factors underlying genome evolution in wild populations, and the consequences of processes such as ILS and introgression on the evolution of phenotypic traits (e.g., Feng et al. 2022).

In sexually reproducing organisms, gene-tree heterogeneity chiefly results from ILS and introgression. The former is a neutral process resulting from the retention of standing variation in nonsister lineages, which depends on the effective population sizes (N_e) and divergence times (Degnan and Rosenberg 2009). Introgression, the transfer of genetic material across lineages through interbreeding, is more difficult to predict because its occurrence depends on the lineages' biogeographic history to include secondary contact for gene flow to occur (Burbrink and Gehara 2018) and that resulting hybrids are reproductively viable. The temporal persistence of introgressed variants depends on

both neutral sorting processes and selection (against or favoring introgressed variants) (Edelman and Mallet 2021). Reproductive isolation increases with divergence between lineages, thus reducing the potential contributions of introgression to gene-tree heterogeneity at deeper evolutionary timescales. Yet introgression has been documented across a range of branch divergence levels in the tree of life, from incipient species to distinct genera (Mallet et al. 2016). Several studies have highlighted the role of introgression in generating novel traits, especially in the context of adaptive radiations (Pease et al. 2016; Svardal et al. 2020; Meier et al. 2023). Consequently, introgression is now recognized as a fundamental and common phenomenon, but the biogeographic context in which it occurs is rarely well understood (Vanderpool et al. 2020).

Gene-tree heterogeneity can result from introgression occurring at early stages of speciation where introgressed alleles persist in present-day populations even in the absence of gene flow. This phenomenon of "ancestral introgression" is well exemplified by reported introgression between strictly allopatric species (e.g., Ferreira et al. 2021) or distantly related lineages with now-complete reproductive isolation (e.g., Rancilhac et al. 2021; Suvorov et al. 2022). By contrast, the impact of contemporary introgression on patterns of gene-tree heterogeneity in parapatric species has garnered little attention (but see Thom et al. 2018). Because gene flow is not homogeneous across space, we expect that the effect of contemporary gene flow on gene-tree genealogies would depend on the geographical sampling considered. More specifically, we hypothesize that the populations furthest away from hybrid zones are less likely to be introgressed, and their relationships should thus reflect the species tree. However, neutral genetic variants may be introgressed far from the contact zone (Payseur 2010; Cruzan et al. 2021). How neutral introgression across hybrid zones can affect the genomic landscape of genealogical variation, and the geographic scale of this phenomenon, has not been documented. Combining hybrid zone analysis with patterns of gene-tree heterogeneity at the scale of the whole genome may provide a powerful tool to address this question. Indeed, geographic clines fitted to allele frequencies at single-nucleotide polymorphisms (SNPs) across the genome provide estimates of local rates of introgression (Dufresnes et al. 2021), which can then be compared with local phylogenetic signals.

In this study, we investigated the contribution of ongoing gene flow to genome-wide phylogenetic conflicts in the red- and yellow-fronted tinkerbirds (*Pogoniulus pusillus–chrysoconus* species group). This group of African barbets has long been recognized as two species (Kirschel et al. 2021), the red-fronted tinkerbird (*P. pusillus*, hereafter RFT) and yellow-fronted tinkerbird (*P. chrysoconus*, hereafter YFT), each of which are further divided into 3 subspecies (RFT: *P. p. affinis*, *pusillus*, and *uropygialis*; YFT: *P. c. chrysoconus*, *extoni*, and *xanthostictus*) with limited or no range overlap between subspecies (Fig. 1). Although recent work suggests that the group may best be treated as 3 or more species (Kirschel et al. 2021), we here follow the traditional two-species partition pending future taxonomic decisions. RFT has a disjunct distribution, with two subspecies in Eastern Africa (*P. p. affinis* and *P. p. uropygialis*) and the nominate form in Southern Africa (*P. p. pusillus*). YFT occupies most of Central and Western Africa, where one lineage found in the northern savanna region contains *P. c. chrysoconus* and *P. c. xanthostictus* with *P. c. extoni* further south (Nwankwo et al. 2019). The YFT subspecies do not form a monophyletic group in previous mtDNA-based reconstructions (Nwankwo et al. 2019; Kirschel et al. 2021). The distribution of taxa in Ethiopia is especially complicated where contact zones exist between *P. c. xanthostictus*, *P. p. uropygialis*, and *P. p. affinis* (Kirschel et al. 2021). As a result, RFT and YFT form an intricate pattern of replacement and contact zones across Africa, in accordance with their ecological preferences: In the north, RFT (*affinis*, *uropygialis*) occupy drier woodland than YFT (*chrysoconus*, *xanthostictus*), whereas the situation is reversed in the south where RFT (*pusillus*) occurs in wet habitats and YFT (*extoni*) in dry woodland and bush. Assessment of the contact zone between the latter two taxa in Southern Africa based on microsatellites (Nwankwo et al. 2019) and whole-genome sequences (Sebastianelli et al. 2024) reported rampant introgression between the two species. Nevertheless, evidence supporting asymmetric assortative mating in red-fronted tinkerbird based on forecrown color (Kirschel et al. 2020), song, or both might mediate reproductive isolation (Sebastianelli et al. 2024). Thus, RFT and YFT provide an ideal system to investigate the contribution of contemporary introgression to gene-tree heterogeneity. We collected whole-genome resequencing (WGS) data of tinkerbirds across Africa to investigate their phylogenetic relationships and patterns of gene-tree heterogeneity in light of secondary contact zones. We further supported the WGS data with double-digest restriction-site–associated DNA sequencing (ddRADseq) across two contact zones to quantify introgression and determine whether support for specific topologies is influenced by high rates of introgression. We then leveraged our understanding of introgression and gene-tree heterogeneity patterns to investigate the role of genes associated with forecrown coloration as barriers to gene flow.

Materials and Methods

Study Design and Genomic DNA Extractions

We investigated the genomic landscape of phylogenetic variation in the *Pogoniulus chrysoconus–pusillus* complex, and the biogeographic processes contributing to phylogenetic discordances. We assembled a WGS data set consisting of previously published Illumina

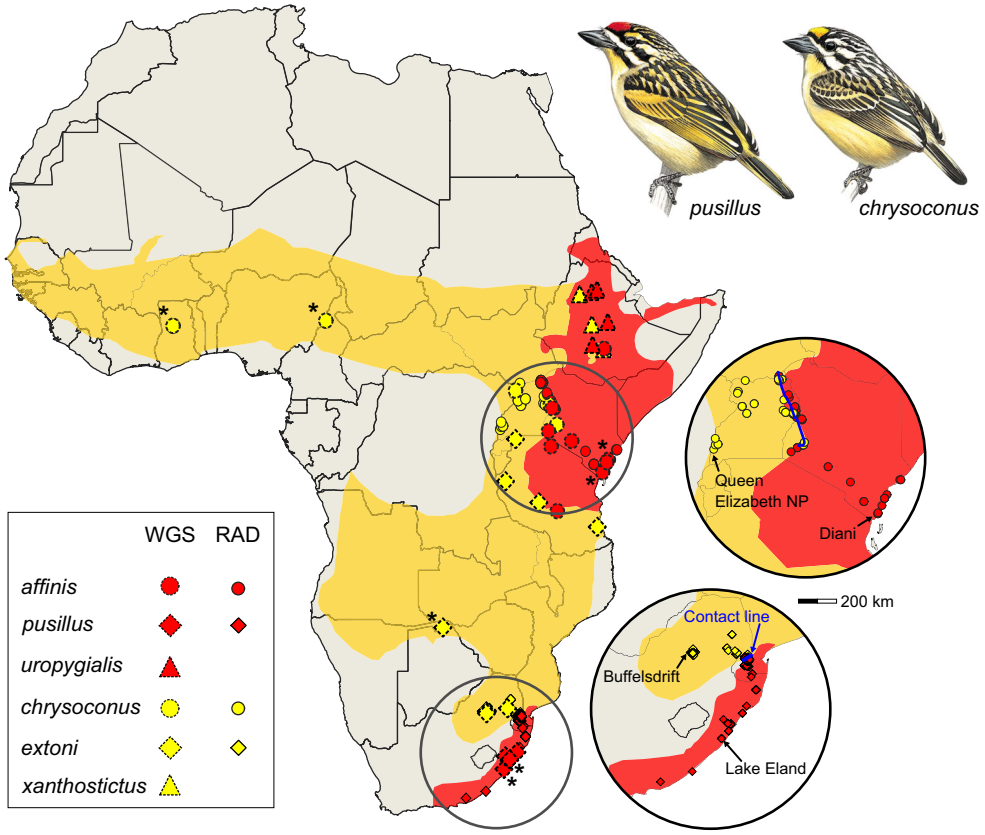

FIGURE 1. Map of the samples used in this study, with the approximate ranges of YFT (yellow) and RFT (red). Markers show sampling locations for the WGS data set (large symbols with dotted contour) and the RADseq data set (small symbols with solid contour). Core range WGS samples are indicated with an "∗". Insets: Details of the contact zones between *P. c. chrysoconus* and *P. p. affinis* in Uganda and Kenya (top) and between *P. c. extoni* and *P. p. pusillus* in Southern Africa (bottom). Markers in the insets detail the sampling used for geographic clines inference (RADseq data only), and solid blue lines show the location of the contact zones. The most distant from the contact zones, used to identify differentially fixed SNPs, are indicated with arrows. (*Note*: For *pusillus*, two localities further away from the contact zone were not included in the single SNP analysis because they were represented by single samples.) Tinkerbird paintings courtesy of del Hoyo et al. (2020).

data from 11 samples from South Africa (Sebastianelli et al. 2024; BioProject PRJNA987636), and 32 newly sequenced samples (Supplementary Table S1; BioProject PRJNA1241442). This sampling covers all taxa in the species complex from both strictly allopatric localities and localities adjacent to contact zones, plus one sample each of the outgroup species *P. atroflavus* and *P. bilineatus*. We additionally collected ddRADseq data sets across two contact zones with the expectation that collected samples represent a range of admixture along geographic transitions: The first contact zone is in Uganda and Kenya for *P. c. chrysoconus* and *P. p. affinis* (108 samples obtained during fieldwork described in Sebastianelli et al. 2022 and Kirschel and Sebastianelli 2022). The second contact zone is in Southern Africa, between *P. c. extoni* and *P. p. pusillus* (525 samples), for which samples were collected and ddRADseq performed previously (see Nwankwo et al. 2019; Kirschel et al. 2020; Sebastianelli et al. 2024). A spreadsheet with metadata for all ddRADseq samples is available as supplementary information (Appendix 1).

We extracted genomic DNA from blood samples for generating the WGS and ddRADseq data sets using a Qiagen DNeasy blood and tissue kit following the manufacturer's protocols (Qiagen, Germany). We quantified DNA on a Qubit 2.0 fluorometer (Thermo Fisher Scientific, Inc.).

WGS Data Set

The WGS data set included 3 RFT subspecies (*P. p. affinis*: $N = 10$, *P. p. pusillus*: $N = 7$, *P. p. uropygialis*: $N = 4$) and 3 YFT subspecies (*P. c. chrysoconus*: $N = 7$, *P. c. extoni*: $N = 10$, *P. c. xanthostictus*: $N = 5$) resequenced at an expected depth of approximately 15-fold coverage (Fig. 1 and Supplementary Table S1). We also included a sample from each of the closely related species *P. atroflavus* and *P. bilineatus* as outgroups. Whole-genome libraries were generated using the NEBNext DNA Library Prep Kit following the manufacturer's recommendations and purified libraries using the AMPure XP system. Each

library was quality checked for size distribution using an Agilent 2100 Bioanalyzer, and quantified using real-time polymerase chain reaction, with paired-end 2 × 150 nt sequence data collected on an Illumina NovaSeq 6000 platform.

We trimmed remnant adapters and clipped low-quality nucleotides (–quality-cutoff 20) using cutadapt v4.0 (Martin 2011) and discarded reads shorter than 20 bp (–minimum-length 20). We next aligned the processed sequence reads to the *P. pusillus* reference genome (GCA_015220805.1) using bwa-mem v0.7.1 (Li and Durbin 2009) and subsequently used SAMtools v1.6 (Danecek et al. 2021) to exclude reads with low mapping qualities (–min-MQ 20), sort the reads by coordinate, and convert to BAM formats. We removed duplicate reads with the MarkDuplicates tool v2.23.1 in Picard (Broad Institute 2019). We recalibrated base quality scores and discovered variants using the following steps, all in GATK v4.2.3 (McKenna et al. 2010): 1) We called genotypes on a per-individual basis with HaplotypeCaller; 2) we combined individual genotypes with CombineGVCFs; and 3) we performed joint genotyping with GenotypeGVCFs . We then used vcftools v0.1.16 (Danecek et al. 2011) to retain only biallelic SNPs with a minor allele frequency (MAF) $\geq$ 0.05, a depth of coverage between 4× and 50×, variants with less than 60% missing data across samples, and quality scores above 20 (–remove-indels –maf 0.05 –minDP 4 –maxDP 50 –max-missing 0.4 –minQ 20 –minGQ 20). In total, we called 112,842,869 autosomal and 11,034,407 Z chromosome SNPs, of which 28,607,336 and 2,886,828, respectively, were retained after filtering.

We inferred the sex of the samples by calculating the ratio of average autosomal depth over average chromosome Z depth, with the expectation that females are half the coverage relative to males (Kirschel et al. 2020; Sebastianelli et al. 2024). In practice, we estimated mean individual depths for chromosome 1 and chromosome Z using vcftools v0.1.16, and calculated ratios using a custom R script. Next, we separated Z chromosome genotypes from male and female individuals in different vcf files, and replaced all heterozygous Z chromosome genotypes from the female vcf with missing data using a custom bash script. Finally, we merged back the males and females using bcftools v1.9 (Danecek et al. 2021), and filtered the sites to remove positions with more than 60% missing genotypes.

Restriction-Site–Associated DNA Sequencing

We generated ddRADseq libraries using the SbfI and MseI restriction enzymes following the protocol described in Brelsford et al. (2016), which includes elements of two previously published protocols (Parchman et al. 2012; Peterson et al. 2012). We used 24 barcoded adapters and 8 indexed primers, which allowed us to pool 192 samples with equimolar concentrations. We collected paired-end 2 × 150 nt sequencing reads on an Illumina HiSeq X Ten platform by Novogene Corporation Inc.

We cleaned sequencing data with subsequent variant discovery for each of the two data sets independently (data set 1: Uganda/Kenya; data set 2: Southern Africa). We demultiplexed each pool using the process_radtags module in Stacks v2.62 (Rochette et al. 2019), discarded reads with uncalled bases (–clean). Cleaned demultiplexed reads are available in dryad (doi:10.5061/dryad.0cfxpnwb3). We aligned the paired-end reads to the *P. pusillus* reference genome (GCA_015220805.1) using bwa-mem v0.7.1. We filtered the resulting SAM files to remove reads with low mapping qualities (–min-MQ 20) using SAMtools v1.6, and then we sorted the reads by their genomic coordinates before converting them to BAM formats. We cataloged SNP loci using the gstacks module and increased the alpha significance thresholds for both SNP discovery (–var-alpha 0.01) and genotype calling (–gt-alpha 0.01).

Phylogenomic Analyses

We used the WGS data set to reconstruct the phylogenetic relationships of the red- and yellow-fronted tinkerbirds. First, we inferred neighbor-joining (NJ) phylogenetic trees in nonoverlapping autosomal and Z chromosome windows using the TopoWindows R script (https://github.com/rancilhac/TopoWindows/tree/main) with a Jukes–Cantor 69 model (Jukes and Cantor 1969). We did not phase SNPs for this analysis, and used windows of 50 SNPs (Martin and Van Belleghem 2017) as well as 500 SNPs to investigate the effect of window size on results. Larger windows may bias the signal toward the commonest topologies, whereas smaller windows may introduce noise due to reduced phylogenetic informativeness in individual windows (Martin and Van Belleghem 2017). All analyses described below were repeated with both window sizes. We used the NJ trees to infer a phylogeny while accounting for ILS with the software ASTRAL. Because ASTRAL assumes free recombination across loci, and no within-loci recombination, we filtered the NJ trees to retain only those corresponding to windows separated by $\geq$10 kb but $\leq$50 kb in size, and used them as input for ASTRAL-II v5.7.8 (Mirarab et al. 2014). We ran this analysis on autosomal and Z chromosome windows separately (birds have a ZW sex chromosome system; Irwin 2018). The 50-SNP autosomal window set was too large for ASTRAL runs to finish in a reasonable time. Thus, we analyzed five random subsets of 15,000 NJ trees and verified that they all yielded the same topology.

Next, we investigated patterns of topological variation using a topology weighting framework, which quantifies the support of a given gene tree *t* to the possible species trees by calculating the proportion of subtrees in *t*, obtained by subsampling a single tip per species, that supports each species tree. Loci under linkage disequilibrium can be included in this analysis, but

within-locus recombination should be avoided. Thus, we retained all NJ trees corresponding to windows ≤50 kb in size and calculated weights using the "complete" method in TWISST (Martin and Van Belleghem 2017). We repeated this analysis on four sets of samples (Supplementary Table S1): 1) all samples; 2) core range samples (>380 km from the contact zones); 3) samples from the contact zones or intermediate with core range (i.e., <300 km from the contact zones); and 4) a set of 14 contact zone samples selected randomly to control variation because of unequal and small sample sizes. As for ASTRAL, we ran TWISST on autosomal and Z chromosome windows, separately.

We incorporated genome-wide recombination rate variation to gain further insights with respect to the processes underlying gene-tree heterogeneity. Regions of low recombination rates should yield more support to the species tree because of reduced local effective population size (N_e) in turn reducing the probability of ILS (Pease and Hahn 2013). Further, in low-recombination region barrier loci have a broader effect, resulting in an underrepresentation of introgressed topologies (Martin et al. 2019). We investigated the relationship between the weight of the 15 possible topologies and local recombination rate. We used estimates of the population recombination rate $\rho = 4N_e \times r$ (with r the recombination rate and N_e the effective population size) in 100-kb windows (Sebastianelli et al. 2024; available as supplementary data) to attribute a recombination rate to each 50- and 500-SNP window. We also used the NJ trees to investigate phylogenetic patterns around the coding sequence of the gene CYP2J19 (chr8: 2377713–2392689), associated with red and yellow forecrown coloration by way of dietary carotenoid conversion (Kirschel et al. 2020). To investigate whether the allele coding for the red-fronted phenotype could have introgressed from one form of RFT to the other, we investigated the length of branches separating *affinis–uropygialis* from *pusillus* in the NJ trees from chromosome 8 (Smith and Kronforst 2013). More specifically, we calculated the average pairwise patristic distance between all combinations of samples from either lineage, which we normalized by dividing with the tree's diameter (i.e., largest pairwise patristic distance in the tree; Mai and Mirarab 2018) to account for general variations in branch length across loci. We compared the distributions of patristic distances in 5 tree sets: total 5 trees overlapping CYP2J19 and lending full support to monophyletic RFT (see results for more details); all 1027 trees lending full support to monophyletic RFT on chromosome 8, and a set of 1027 random trees from chromosome 8 as a basis of comparison. We calculated patristic distances using a custom R script based on adephylo v1.1-13 (Jombart and Dray 2010).

Finally, we inferred genome-wide patterns of introgression by calculating *f*-branch statistics based on the autosomal data using Dsuite v0.5r52 (Malinsky et al. 2021) and polarized using the autosomal topology obtained with ASTRAL from low-recombination regions (cf. results for more details). In order to investigate the relationship between introgression and recombination rates, we calculated the f_{dM} statistic (Malinsky et al. 2015) in nonoverlapping windows of 50 SNPs for two taxa trios that minimized the likelihood of introgression between both P2–P3 and P1–P3: ((P1 = *pusillus*, P2 = *chrysoconus–xanthostictus*), P3 = *extoni*) (our results suggest minimal or nonexistent introgression between the latter two) and ((P1 = *affinis–uropygialis*, P2 = *pusillus*), P3 = *chrysoconus–xanthostictus*) (geographic ranges, and our genomic analyses, support no introgression between the latter two).

Analyses of Contact Zones

To better understand patterns of introgression, we performed geographic cline analyses across the *P. c. chrysoconus* versus *P. p. affinis* and *P. c. extoni* versus *P. p. pusillus* contact zones using the ddRADseq data sets. We first investigated changes in genome-wide individual ancestry-proxies along geographic gradients across the contact zones. Lines best representing the center of the contact zones were drawn in ArcGIS v10.7 based on where the two forecrown feather color phenotypes were in approximately equal frequency, and the shortest distance to the line was calculated for each sample. By convention, we considered the contact line as the "0 km" point in the geographic gradient, and negative geographic distances in the RFT side of the contact zone (i.e., either *P. p. affinis* or *P. p. pusillus*). For each sample, we estimated genome-wide ancestry-proxies using ADMIXTURE v1.3 (Alexander et al. 2009) with default parameters and two assumed ancestral parental populations ($K = 2$). For this analysis, we used the *populations* module in Stacks to generate vcf files from the outputs of *gstacks*. We filtered SNP loci with vcftools v0.1.16 to keep only biallelic sites with an MAF ≥ 0.05, a minimum depth of coverage of 3×, a mean maximum depth of coverage of 24×, and less than 30% missing data (–min-alleles 2 –max-alleles 2 –maf 0.05 –minDP 4 –maxmeanDP 24 –max-missing 0.7). We used HZAR v0.2-5 (Derryberry et al. 2014) to fit sigmoid clines to the transition in individual RFT ancestry-proxies along the geographic gradient. We tested four cline models differing by the presence of introgression tails modeling neutral gene flow: 1) tails on either side of the cline, which can be asymmetrical; 2) a single tail on the left side; 3) a single tail on the right side; or 4) no tail at all. As the populations most distant from the contact zones were not admixed (i.e., RFT ancestry = 0.0 or 1.0), we did not test models with free maximum and minimum ancestry. We also tested a null model corresponding to no changes in ancestry. We used the corrected Akaike information criterion to determine the best-fit models. We repeated this analysis for each of the contact zone data sets. We next estimated per-SNP clines based on allele frequencies to test whether the variation in phylogenetic signal across the genome could be linked to variations in the rates of

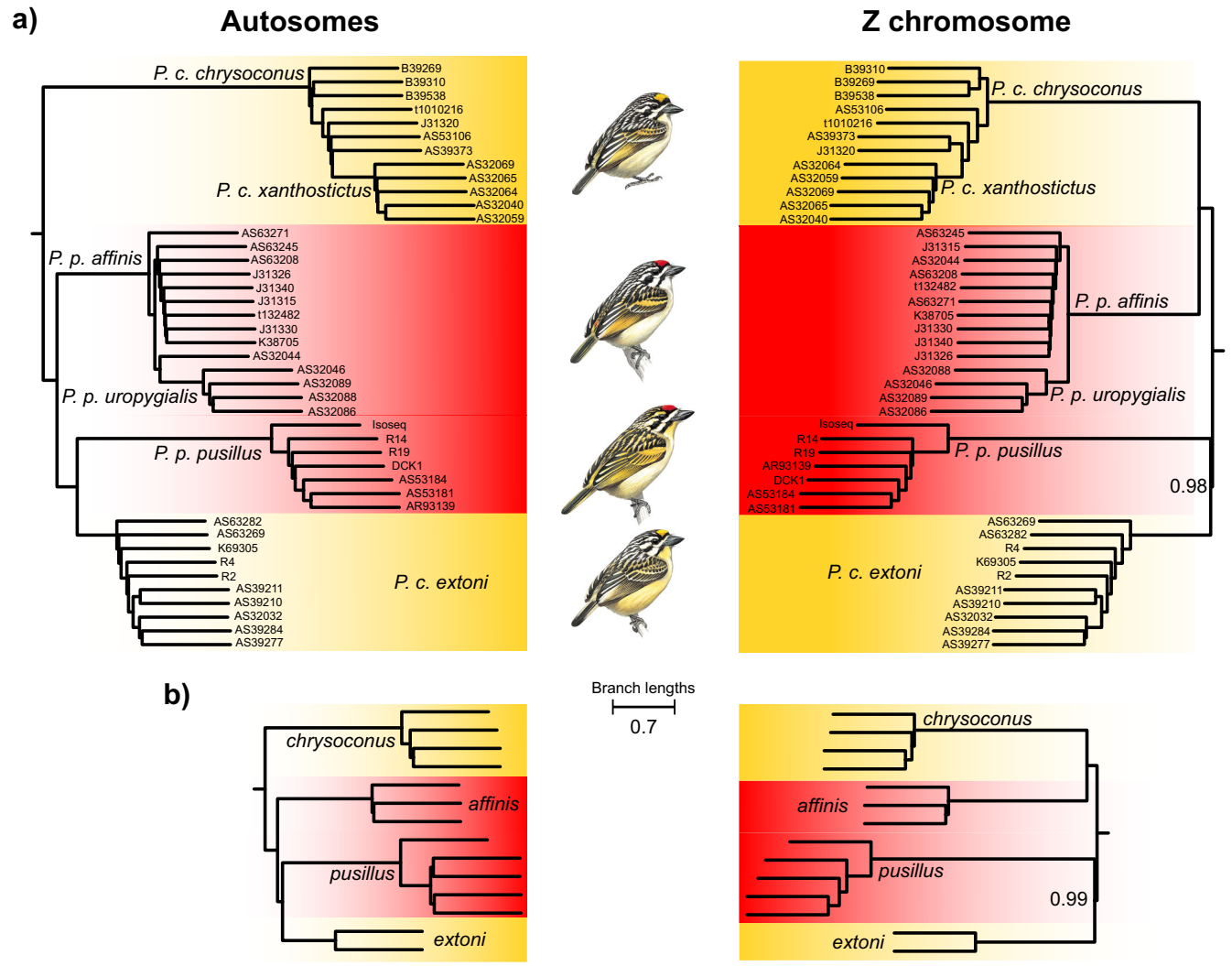

FIGURE 2. Species trees estimated using ASTRAL based on NJ trees reconstructed in nonoverlapping sliding windows of 50 SNPs using a) autosomal (left; 15,000 randomly selected trees) and Z chromosome (right; 8523 trees) data from all samples and b) autosomal (left; 15,000 randomly selected trees) and Z chromosome (right; 8524 trees) data from "core range" samples only. All internal nodes received a PP = 1.0, except for two nodes in the Z chromosome phylogenies, for which the PP is indicated. Support for nodes within each lineage is not represented for improved clarity. The trees were rooted with sequences of *P. atroflavus* and *P. bilineatus*, not represented for improved clarity. Branch lengths reflect coalescence units. Tinkerbird paintings courtesy of del Hoyo et al. (2020).

introgression. Based on the output of *gstacks*, we used the *population* module in Stacks to retain only a single SNP per RAD locus (–write-random-snp) and report allele frequencies at each locality (–hzar). Because estimating allele frequencies requires several individuals, localities represented by single samples were lumped with neighboring localities. We obtained sets of 97,501 and 97,536 SNPs in the southern and northern hybrid zones, respectively. We subsequently filtered them to keep only those that 1) were genotyped in at least two samples in each locality and 2) were differentially fixed in the two extreme localities of the geographic gradient (diagnostic SNPs), resulting in 1852 SNPs for the southern hybrid zone and 5378 for the northern hybrid zone. We used the resulting SNP sets to model changes in allele frequencies across geographic gradients crossing the contact zones at each locus using the same approach as described above.

RESULTS

Pervasive Gene-Tree Heterogeneity in the Red- and Yellow-Fronted Tinkerbird Radiation

We first inferred evolutionary relationships of the red- and yellow-fronted tinkerbirds using the WGS data. We inferred gene trees in nonoverlapping windows and reconstructed the species relationships separately for autosomal and Z chromosome windows while accounting for ILS. Analyses of autosomal windows of both 50 and 500 SNPs yielded a fully supported topology (posterior probability [PP] of all internal nodes = 1.0) (Fig. 2a and Supplementary Fig. S1a) dividing the red- and yellow-

fronted tinkerbirds into four main lineages: *P. c. chrysoconus* (with *P. c. xanthostictus* nested within), *P. c. extoni*, *P. p. affinis* (with *P. p. uropygialis* nested within), and *P. p. pusillus*. Because species limits do not seem to agree with the traditional two-species taxonomy (Kirschel et al. 2021; this study), we hereafter refer to them as *chrysoconus–xanthostictus*, *extoni*, *affinis–uropygialis*, and *pusillus*, to refer to the northern and southern forms of YFT and RFT, respectively. The autosomal topology placed *chrysoconus–xanthostictus* as sister to the other lineages and *affinis–uropygialis* as sister to a monophyletic *pusillus* + *extoni*. Both *uropygialis* and *xanthostictus* were monophyletic within their respective clade and separated by relatively long branches. We repeated this analysis with a subset of 14 samples from core range localities (i.e., >380 km away from contact zones; hereafter "core range" samples) and found the same relationships (Fig. 2b and Supplementary Fig. S1b). Contrastingly, the Z chromosome produced two different topologies, depending on whether windows of 50 or 500 SNPs were used. In the former, northern (*chrysoconus–xanthostictus* and *affinis–uropygialis*) and southern (*extoni* and *pusillus*) taxa formed two reciprocally monophyletic groups (Fig. 2a), whereas in the latter, *pusillus* was sister to the northern taxa (Supplementary Fig. S1a), although with low support. When analyzing only "core range" samples, however, both window sizes yielded the former topology, with reciprocally monophyletic northern and southern taxa (Fig. 2b and Supplementary Fig. S1b). All of our reconstructed topologies were discordant with the mtDNA relationships inferred by Nwankwo et al. (2019).

Next, we explored the extent to which gene-tree heterogeneity exists in the red- and yellow-fronted tinkerbird genomes using a topology weighting approach. Based on our genome-wide phylogenetic reconstructions, we merged the *uropygialis* subspecies with *affinis* and separately the *xanthostictus* subspecies with *chrysoconus* to reduce the space of possible species trees. Thus, there are 15 possible rooted species tree topologies, hereafter referred to as topologies T1–T15 (Supplementary Table S2). We hereafter described results based on windows of 50 SNPs, and those based on windows of 500 SNPs are presented in the supplementary material. We also provide information about the size and number of windows in each set in Supplementary Table S3. For both autosomes and Z chromosome, we uncovered important topological heterogeneity with all 15 possible topologies supported (Fig. 3a and Supplementary Table S2). In autosomal windows, five topologies had an average weight >8% in decreasing order of frequency: the topology obtained from the autosome-based phylogenetic inference (T15, 15.98%); ((*affinis–uropygialis*, *chrysoconus–xanthostictus*), (*extoni*, *pusillus*)) (T3, 10.11%); (((*affinis–uropygialis*, *chrysoconus–xanthostictus*), *extoni*), *pusillus*) (T1, 9.62%); (*chrysoconus–xanthostictus*, (*pusillus*, (*affinis–uropygialis*, *extoni*))) (T5, 9.52%); and (*chrysoconus–xanthostictus*, (*extoni*, (*pusillus*, *affinis–uropygialis*))) (T8, 9.35%). These topologies all support pairs of monophyletic lineages that also have a contact zone, except for T8 in which RFT is monophyletic (Supplementary Table S2).

Plumage colouration appeared to be a poor predictor of phylogenetic relationships. The topologies that supported RFT as monophyletic had relatively low frequencies (T7, T8, and T9; cumulative average weight of 16.94%) and YFT was even less supported as monophyletic (T9, T12, and T13; cumulative average weight of 9.25%). Topological variation on the Z chromosome was very distinct from that of autosomes (Fig. 3a). There, the most commonly supported topologies were T1 (10.39%), T3 (9.41%), and (*extoni*, (*pusillus*, (*affinis–uropygialis*, *chrysoconus–xanthostictus*))) (T2, 8.35%). All three of these topologies supported *affinis–uropygialis* as sister species to *chrysoconus–xanthostictus*. Topology T15 (8.09%) was the only other topology with an average weight >8.00% on the Z chromosome. The most striking difference between the autosomes and the Z chromosome was the support for T15, which dropped from 15.98% in the former to 8.09% in the latter. As in the autosomes, the topologies where RFT was monophyletic were more frequent than those where YFT was monophyletic (cumulative average weights of 20.09% vs. 13.47%, respectively).

In the autosomes, we did not find large contiguous blocks of windows supporting the same topology. Instead, these windows were dispersed along the chromosomes, interspersed with windows supporting other topologies (Fig. 4a and Supplementary Fig. S2). Contrastingly, on the Z chromosome, we identified four contiguous blocks of windows spanning 2.70–6.40 Mb with a high support for T1 and T3 (Supplementary Fig. S2). The cumulative support for monophyletic RFT topologies was also higher on the Z chromosome compared with the autosomes, especially within a 3.50-Mb block where they were the most supported topologies.

We classified 1) whether the topologies were concordant according to forecrown plumage coloration or 2) whether at least one pair of taxa with a contact zone were sister lineages (hereafter "geography") (Supplementary Table S2). The "geography" category dominated the signal with cumulative average weights of 68.39% and 59.78% in the autosomes and Z chromosome, respectively (Fig. 3b and Supplementary Figs. S3 and S4). To determine whether these levels of heterogeneity could be recovered even when considering only samples from localities far away from the contact zones, we partitioned the data set into two subsets, "core range" (14 samples) and "contact zones" (29 samples), and repeated the analysis. Considering the imbalance in sample size where most samples were located proximal to the contact zones, we also generated a "control" subset of 14 samples from the contact zones to match the sample size of the "core range" subset. The "contact zones" subset produced nearly identical results as the complete set; however, two monophyletic RFT topolo-

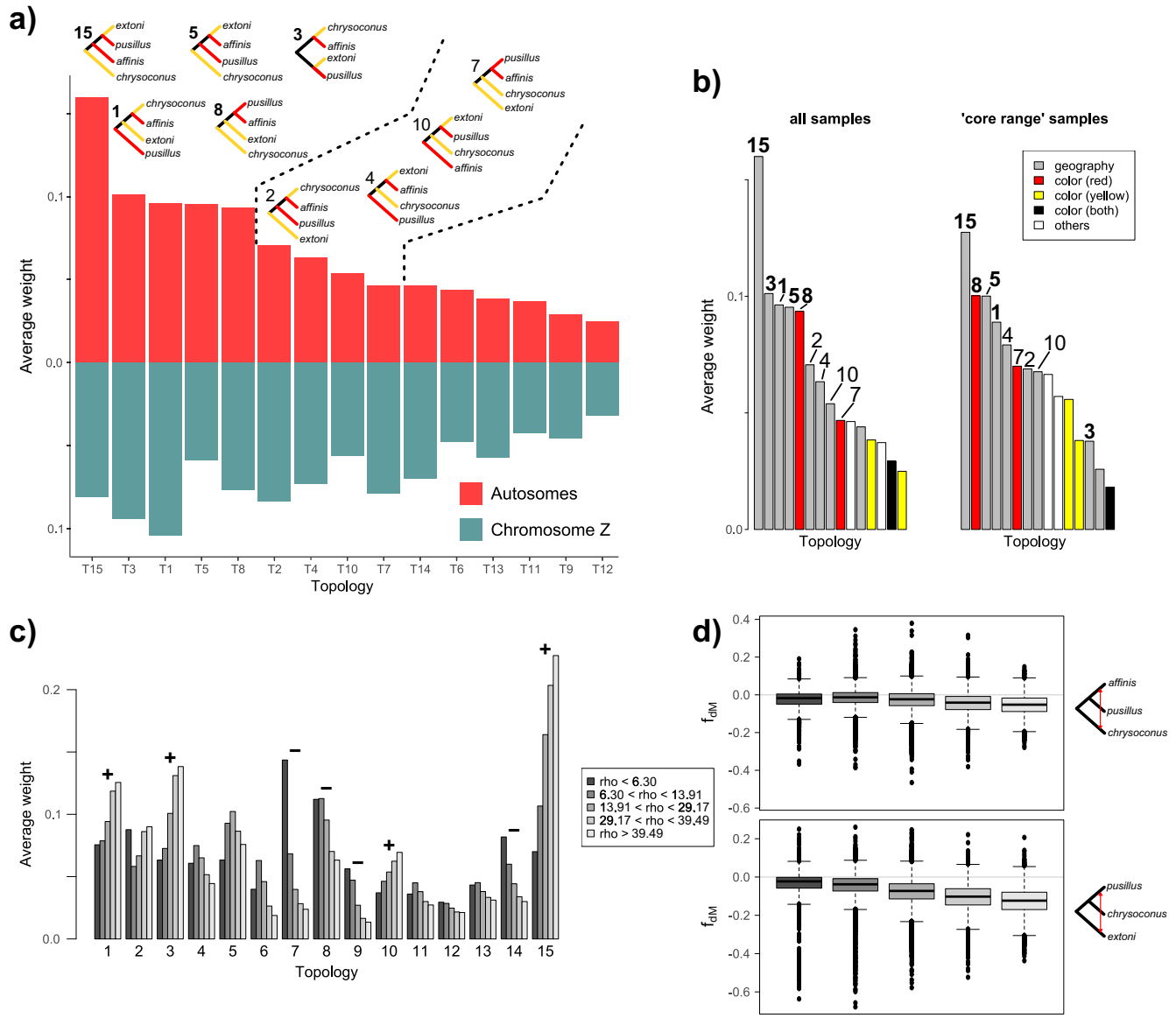

FIGURE 3. Results of topology weighting analyses. a) Average weight for each of the 15 possible species trees in the autosomes (top bars) and Z chromosome (bottom bars). The topologies are ordered based on their support in the autosomal analysis, and the nine with the highest average weight are illustrated. b) Autosomal results based on two sample subsets: all samples (left barplot, same as red bars in panel a) and 14 "core range" samples collected far from the contact zones. The topologies are colored according to one of five categories defined based on the taxa supported as monophyletic (see Supplementary Table S2 for more details). c) Variation of the average weigh in autosomal windows t at each topology depending on the recombination rate (represented here as the population recombination rate, rho). Windows were divided into five categories corresponding to the 0–5%, 5–20%, 20–80%, 80–95%, and 95–100% quantiles of the recombination rate distribution. Symbols above the bars denote topologies that either increase (+) or decrease (−) in support with increasing recombination rate. d) Association between introgression (measured with the f_{dM} statistic) and recombination rates. Dendrograms on the right show the trios being tested (P1, P2, and P3 ordered from top to bottom). A negative f_{dM} means introgression between P1 and P3 (shown as a red arrow in the dendrograms).

gies (T7 and T8) in the "core range" subset increased substantially in frequency in both autosomal and Z chromosome analyses (Fig. 3b and Supplementary Fig. S3). The "contact zones" control subset showed that with a reduced sample size, even when using samples from the contact zones, T7 and T8 were more frequent than when using all the samples (Supplementary Figs. S3 and S4). Importantly, the mean weight of T7 and T8 was significantly higher when using the "core range" samples compared with the control subset (Wilcoxon rank sum test $P < 2.20 \times 10^{-16}$ in both cases). Despite these differences, T15 was the dominant topology in the autosomes and T1 and T3 in the Z chromosome data, with considerable gene-tree heterogeneity in all analyses.

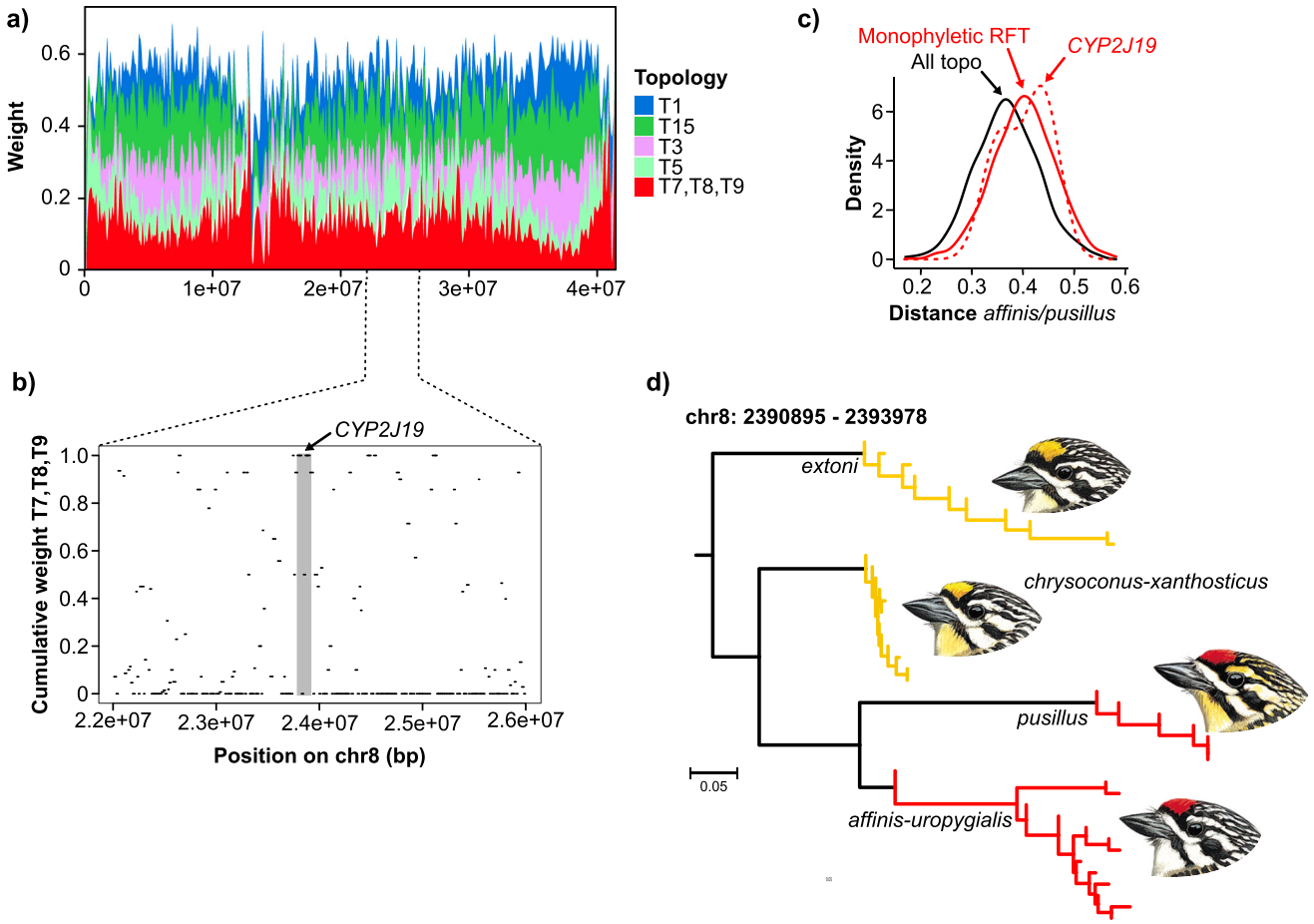

FIGURE 4. Phylogenetic signal on chromosome 8. a) Distribution of the weights of the four commonest topologies (T1, T3, T5, and T15) as well as cumulative weights of the topologies where red-fronted tinkerbirds are monophyletic (T7, T8, and T9) along chromosome 8. The weights were smoothed using a local regression with a span of 0.01. b) Zoom into the region surrounding the gene CYP2J19 (gray rectangle shows the gene), with the horizontal bars representing the cumulative weight of T7, T8, and T9 in each 50-SNP window. c) Distribution of the length of branches separating *affinis–uropygialis* from *pusillus* in 1027 random NJ trees supporting any topology (black line), all 1027 trees with a cumulative weight for T7,T8,T9 = 1.00 on chromosome 8 (solid red line), and the 5 trees overlapping CYP2J19 with a cumulative weight for T7,T8,T9 = 1.00 (dashed red line). Branch length is represented as the average pairwise patristic distance between all samples of either RFT lineages, normalized by the diameter of the tree. d) Example of a NJ phylogenetic tree from a window overlapping CYP2J19. Tinkerbird paintings courtesy of del Hoyo et al. (2020).

Monophyly among Parapatric Lineages Overrepresented in High Recombination Rate Regions

When considering only regions with very low recombination rate (population recombination rate [ρ] < 6.30, corresponding to the 5% quantile of ρ), the monophyletic RFT topologies T7 (sister to *chrysoconus*) and T8 (sister to *extoni*) were the most common (average weights of 14.4% and 11.2%, respectively; Fig. 3c). With increasing recombination rate, their proportion rapidly decreased, whereas some topologies that included geographically proximate populations increased (e.g., T1 with northern *affinis* and *chrysoconus* sister, T3 with both northern and southern geographically proximate RFT and YFT sister taxa, and T10 and T15 with *extoni* and *pusillus* sister). For four topologies, support decreased with increasing recombination rate: T7, T8, T9, and T14. T2 also decreased in the first three categories, but slightly increased in the highest recombination rate categories. Topologies T7, T8, and T9 supported RFT as monophyletic, and topologies T2, T7, and T14 supported *extoni* as sister to the remaining taxa. On the contrary, three topologies showed a strong increase in frequency: T1, T3, and T15. These all supported *pusillus* + *extoni*, *affinis–uropygialis* + *chrysoconus–xanthostictus*, or both, as monophyletic. We subsequently used windows with the lowest recombination rate for phylogenetic reconstruction and found that topology T7 was fully supported (Supplementary Fig. S5), which is concordant with mitochondrial relationships (Nwankwo et al. 2019; Kirschel et al. 2021) and suggests a monophyletic RFT.

Introgression analysis using the *f*-branch statistic based on topology T7 (Supplementary Fig. S6) supported significant introgression between *affinis–uropygialis* and *chrysoconus–xanthostictus* (f_b = 0.08, Z

score = 80.70) as well as between *extoni* and the ancestral branch of RFT ($f_b = 0.29$, Z score = 114.45). We attribute the latter to parallel introgression between *extoni* and both *affinis* and *pusillus* through the hybrid zones in Tanzania and South Africa, respectively. Furthermore, in the trios ((P1 = *pusillus*, P2 = *chrysoconus–xanthostictus*), P3 = *extoni*) and ((P1 = *affinis–uropygialis*, P2 = *pusillus*), P3 = *chrysoconus–xanthostictus*), we found that the f_{dM} statistic was negatively correlated with recombination rate (Fig. 4d and Supplementary Fig. S7; Spearman rank correlation test $P < 2.20 \times 10^{-16}$, $\rho = -0.35$ and -0.21, respectively). A negative f_{dM} indicates introgression between P1 and P3.

We explored the phylogenetic signal around the gene *CYP2J19*, underlying red and yellow colorations (Kirschel et al. 2020), to investigate whether it supported a single origin of red forecrown, as suggested by our preferred species tree hypothesis. We found that 7 of the 9 windows overlapping *CYP2J19* (chr8: 2377713–2392689) supported monophyletic RFT (i.e., cumulative weight of T7, T8, and T9 > 0.9). Contrastingly, 174 out of 194 windows flanking the gene (i.e., 250 kbp downstream or upstream the coding region) supported paraphyly for RFT (Fig. 4b). Only 10 windows upstream and 13 downstream carried a weight >0.80 for T7, T8, and T9 considered together. Samples of *affinis–uropygialis* and *pusillus* were separated by long branches in the windows supporting monophyletic RFT overlapping *CYP2J19* compared with other windows on chromosome 8, suggesting an old divergence at this locus rather than recent introgression (Fig. 4c).

Topology weighting analyses of 500-SNP windows yielded similar patterns, although support for the commonest topologies was proportionally increased, and vice versa for the rarest ones, consistently with a reduction of phylogenetic noise owing to increased informativeness of individual windows (Supplementary Figs. S8–S11). This was also verified when considering the proportion of fully resolved windows (i.e., lending a weight = 1 to a given topology), a more stringent measure of phylogenetic support compared with mean weight.

Levels of Introgression across Contact Zones Are Associated with Phylogenetic Signal

Our analyses suggest that RFT taxa *pusillus* and *affinis–uropygialis* are sister lineages, and that introgression between parapatric lineages generated high levels of phylogenetic heterogeneity. It remains unclear, however, whether these patterns of introgression are the legacy of ancestral (i.e., at the first stage of contact) or contemporary gene flow. To clarify this, we used the ddRADseq data set to study transitions in genomic ancestry and allele frequencies along geographic gradients that cross two contact zones: between *chrysoconus* and *affinis* (in Uganda and Kenya), and between *extoni* and *pusillus* (in Southern Africa). Summary statistics of the two data sets are given in Supplementary Table S4. Clines fitted to ancestry-proxies (i.e., Q values) were narrow (Fig. 5a,b; cline parameters are detailed in Supplementary Table S5), with widths of 10.00 km (95% CI [6.80, 15.60]) for the *chrysoconus* versus *affinis* cline in the north and 4.30 km (95% CI [1.20, 14.20]) for the *extoni* versus *pusillus* cline in the south. However, we inferred bidirectional introgression tails in the latter, which suggested neutral introgression, with admixed individuals found >30 km from the contact zone. By contrast, the northern contact zone was best modeled by a simple cline without introgression tails.

We next fitted sigmoid clines to the transitions in allele frequencies at diagnostic SNPs (i.e., SNPs that are differentially fixed in the populations most distant from the contact zone) and tested whether some topologies were associated with wider clines than others. If patterns of gene-tree heterogeneity are the result of contemporary gene flow, we predict that genomic regions supporting taxa with a contact zone as monophyletic would also harbor SNPs with wider clines. Conversely, clines should be narrower in regions supporting the putative species tree topology (with *affinis–uropygialis* and *pusillus* as sister lineages). In Southern Africa (*extoni* vs. *pusillus* transition), the mean width of single-locus clines was 65.23 ± 144.09 (SD) km (range = 1.30–999.80 km) (Fig. 5c). We compared cline widths at SNPs located in genomic regions that supported three categories of topologies: *extoni* + *pusillus* as sister taxa (topologies T3, T10, and T15); any other taxa pair as sister taxa (i.e., all other topologies except the aforementioned three); and specifically *affinis–uropygialis* and *pusillus* as sister taxa (topologies T7, T8, and T9, also included in the previous category). We found that SNPs in the *extoni* + *pusillus* category followed significantly wider clines (mean width = 63.81 km) than those in the other two categories (width = 43.80 and 33.66 km; Wilcoxon rank sum test $P = 2.50 \times 10^{-6}$ and 7.43×10^{-6}, respectively), even when we removed outlier loci (i.e., clines with a center >100 km away from the contact zone or a width >300 km) (Fig. 5e and Supplementary Fig. S12). Across the Uganda/Kenya contact zone (*chrysoconus* vs. *affinis* transition), single-locus clines were significantly narrower (mean 25.39 ± 67.43 [SD] km, range = 0.30–1080.80 km) than in Southern Africa (Wilcoxon rank sum test $P < 2.20 \times 10^{-16}$) (Fig. 5d). Again, we divided the SNPs in three categories depending on local phylogenetic support (*chrysoconus* + *affinis*: topologies T1, T2, and T3; all other topologies; and *affinis* + *pusillus* only). SNPs in the *chrysoconus* + *affinis* category did not follow significantly wider clines than those in the "all other topologies" category (mean widths = 23.86 and 22.84 km, Wilcoxon rank sum test $P = 0.24$) (Fig. 5f and Supplementary Fig. S13); however, clines in the *affinis* + *pusillus* category were narrower (mean width = 22.27 km, $P = 0.025$). In both contact zones,

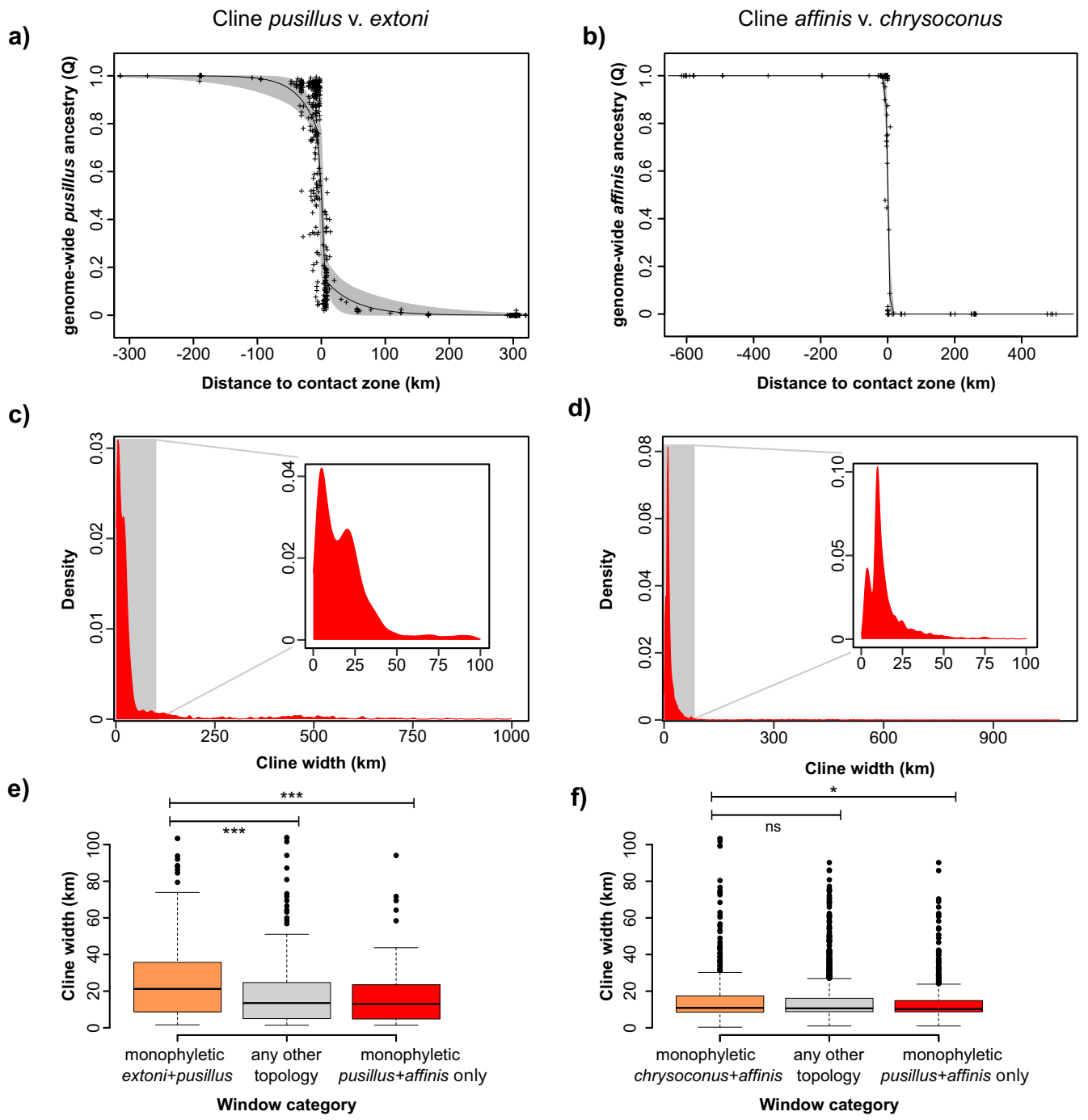

FIGURE 5. Results of cline analyses across the *extoni* versus *pusillus* (a, c, e) and the *chrysoconus* versus *affinis* (b, d, f) contact zones. a, b) Sigmoid clines fitted to genome-wide individual ancestry-proxies (*Q* values) calculated using ADMIXTURE, represented as black crosses. Black lines show the maximum likelihood cline, and the gray envelope the 95% credibility parameter space. c, d) Density plots of the distribution of cline widths in single-locus analyses. Insets show density distributions for loci with a cline width ≤100 km. e, f) Distribution of cline widths in genomic regions supporting three categories of topologies (from left to right): topologies supporting species with a contact zones (i.e., either *chrysoconus–xanthostictus* + *affinis–uropygialis* or *extoni* + *pusillus*) as monophyletic; topologies supporting any other taxa pair as monophyletic ("all others", includes 12 topologies); and of the latter, those specifically supporting *pusillus* + *affinis–uropygialis* as monophyletic (T7, T8, and T9). *Note*: The *y*-axes ranges were shortened to 100 km to improve visualization; however, the statistical analysis was run on the complete data range.

we found similar associations when using weights calculated in 500-SNP windows (Supplementary Figs. S14–S16). The major difference was that in the *chrysoconus* versus *affinis* transition, SNPs in the *chrysoconus* + *affinis* category had significantly wider clines than SNPs in the "all other topologies" and *affinis* + *pusillus* categories (Supplementary Fig. S16). Finally, we found a positive correlation between cline width and recombination rate in both contact zones (Spearman rank correlation test $P < 2.20 \times 10^{-16}$, $\rho = 0.28$ and 0.47) (Supplementary Fig. S17).

Discussion

Gene flow and admixture have a crucial role in evolution, both as forces counteracting local adaptation and divergence (Kawecki and Ebert 2004) and as sources of novel allele combinations fueling diversification (Meier et al. 2023). The temporal stage at which such genetic exchange occurred is critical to understanding how barriers to gene flow evolve and shape genome-wide divergence. In this study, we investigated introgression in red- and yellow-fronted tinkerbirds (*Pogoniulus pusillus–chrysoconus* species group), a complex of closely related barbets with intricate secondary contact zones across Africa (Nwankwo et al. 2019; Kirschel et al. 2020; Kirschel and Sebastianelli 2022; Sebastianelli et al. 2024), by characterizing patterns of phylogenomic variation. We analyzed genome-wide SNPs in a framework accounting for ILS and generated an initial phylogenetic hypothesis where neither currently recognized species was monophyletic. Instead, the yellow-fronted *P. c. chrysoconus* split earliest in the radiation, followed by the red-fronted *P. p. affinis*, which was sister to two forms from Southern Africa (red-fronted *P. p. pusillus* and yellow-fronted *P. c. extoni*) that are geographically adjacent to one another. The subspecies *P. c. xanthostictus* and *P. p. uropygialis* were nested within *P. c. chrysoconus* and *P. p. affinis*, respectively. Although this topology was fully supported, the phylogenetic relationships of these four lineages varied across the genome. Topologies placing taxa with a secondary contact zone as sister to each other (e.g., *chrysoconus* + *affinis*, *extoni* + *affinis*, and *extoni* + *pusillus*) were supported by 80% of the genomic windows. The only exception was the pair of yellow-fronted *chrysoconus* + *extoni*, which presumably have been in recent contact in Uganda (Kirschel and Sebastianelli 2022) yet were seldom monophyletic (cumulative average weight of 9.25%). By contrast, RFT were more frequently recovered as monophyletic. This discord between phenotypic similarity and genome-wide phylogenetic signal suggests either parallel evolution of red and yellow forecrown coloration or a genome-wide erosion of the phylogenetic support for the species tree, i.e., due to introgression.

Neutral Gene Flow through Narrow Hybrid Zones Shapes Gene-Tree Heterogeneity

The extent of phylogenetic heterogeneity across the genome as a consequence of introgression depends on the biogeographic history of the populations, as well as processes acting on the genome, in particular natural selection and genetic recombination (Burbrink and Gehara 2018; Musher et al. 2024; Thom et al. 2024). Theory predicts that a positive correlation between introgression and recombination rate is produced when introgressed alleles are purged by selection (Schumer et al. 2018; Martin et al. 2019; Duranton and Pool 2022). Such a correlation has been used to identify local phylogenetic signals that likely result from introgression (Li et al. 2019; Hennelly et al. 2021; Foley et al. 2024; Jiang et al. 2024). We found that the phylogenetic relationships across RFT and YFT were strongly associated with recombination rate, where genomic windows of lower recombination rates supported the monophyly of RFT. By contrast, three of the dominant topologies in the genome-wide analyses (T1, T3, and T15) were relatively rare in windows characterized by low recombination rates, and their frequencies were strongly positively correlated with recombination rate. It should be noted that a negative relationship between introgression and recombination rate could potentially arise, particularly when the introgressed alleles are under positive selection (Duranton and Pool 2022; Feng et al. 2024). However, our data showed a positive correlation, supporting that introgressed variants are mostly neutral or selected against. Regions of low recombination supported a topology where *P. c. extoni* splits first, and *chrysoconus–xanthostictus* are sister to a monophyletic RFT. We believe this best represents the red- and yellow-fronted tinkerbirds species tree and introgression between parapatric lineages drives gene-tree heterogeneity, even in geographically distant core populations.

We modeled changes in genome-wide ancestry-proxies (Q values) for two of the contact zones and estimated cline widths of 4–10 km, with such narrow transition zones comparable to other avian systems where strong reproductive isolation has been inferred (Price 2008; Grossen et al. 2016; Pulido-Santacruz et al. 2018). As cline width depends on dispersal rates and selection against hybrids, a narrow cline reflects strong reproductive isolation (Barton and Hewitt 1985; Payseur 2010; Dufresnes et al. 2021). Despite that, we detected introgressed alleles hundreds of kilometers away from both contact zones. As reproductive barriers build up across a genome, the distribution of cline width at independent loci is expected to change from a normal distribution to a Poisson distribution, and finally a bimodal distribution where many loci are impermeable to gene flow (Dufresnes et al. 2021). Here, we report distributions of cline widths similar to Poisson distributions, with the emergence of two modes at lower widths. Furthermore, a model with introgression tails best

represented the *extoni* versus *pusillus* transition, consistent with neutral introgression far from the contact zone (Szymura and Barton 1986). Thus, despite narrow transitions in ancestry-proxies, tinkerbird hybrid zones appear porous to neutral introgression, a conclusion that is further supported by the positive relationship between cline width and recombination rate (Duranton and Pool 2022). Introgression dynamics differed across the two contact zones analyzed. The absence of introgression tails in the *chrysoconus* versus *affinis* genome-wide analysis and relatively narrower single SNP cline widths suggests an overall lower rate of introgression in their contact zone, consistent with the phylogenetic analyses that support *extoni* and *pusillus* as sister lineages.

Phylogenetic Signal for the Species Tree Is Conserved in Small, Interspersed Genomic Regions

In both contact zones, the genomic regions that supported parapatric taxa as monophyletic also produced wider transitions in allele frequencies. Because we considered markers that are differentially fixed in allopatric populations on both sides of the contact zone, intermediate allele frequencies along the transect are maintained by ongoing gene flow rather than ancient admixture. Further support is that topology T15 remains dominant even when only allopatric samples were considered, with the *extoni* versus *pusillus* ancestry cline revealing broad introgression tails. Thus, our phylogenomic and geographic cline analyses draw a coherent picture where the dominant phylogenetic signal results from contemporary introgression across contact zones, whereas support for the species tree is conserved in small and interspersed genomic regions. In the *chrysoconus* versus *affinis* contact zone, two topologies that do not support *chrysoconus–xanthostictus* + *affinis–uropygialis* as monophyletic (T5 and T15) were associated with wide clines; however, these topologies are overrepresented in regions of medium or high recombination rate, respectively, which are more permeable to introgression in general. Considering that there are several parallel RFT and YFT hybrid zones across Africa, phylogenetic signal at a given locus must depend on the relative strength of introgression in the different hybrid zones. In this specific case, T5 supports *extoni* + *affinis–uropygialis* as monophyletic, and T15 *extoni* + *pusillus*. Although we did not focus specifically here on the *extoni* versus *affinis* transition, we found that introgression between *extoni* and *pusillus* was stronger than between *chrysoconus* and *affinis*, consistent with the hypothesis that T15 overrides phylogenetic signals in many regions with high recombination rate. Finally, one limitation of our approach is that we could not take recombination breakpoints into account when inferring trees; thus, these local phylogenies may not accurately represent the evolutionary relationships of haplotypes (Martin and Van Belleghem 2017). Consequently, a given local phylogeny likely reflects the dominant signal of introgression in the corresponding genomic window if it overlaps several haplotypes. This may also result in an underestimation of ancient introgression compared with contemporary gene flow as recombination gradually breaks down introgressed haplotypes (Racimo et al. 2015). However, the overall concordance of results based on windows of 50 and 500 SNPs supports that window size does not affect our main conclusions.

Introgression across species is commonly reported in phylogenomic studies (Mallet et al. 2016; Hibbins and Hahn 2022), including cases where the dominant phylogenetic signal results from introgression (Fontaine et al. 2015; Zhang et al. 2021). Here, we show that neutral introgression through narrow secondary contact zones contributes to gene-tree heterogeneity, to a point that introgressed topologies are vastly dominant, even in the species' core ranges. This is consistent with a study on the suboscine bird radiation (Singhal et al. 2021), where range overlap was among the main predictors of the levels of introgression. However, there are examples of closely related, parapatric lineages that do not show introgression (Pulido-Santacruz et al. 2020; Sarver et al. 2021; Khan et al. 2024), whereas deeply diverged parapatric lizard species do (Caeiro-Dias et al. 2021). In that context, the nature of reproductive barriers may be the most important factor constraining introgression, and thus shaping the genomic landscape of gene-tree heterogeneity. Because of that, introgression must be carefully taken into account when reconstructing the phylogenetic relationships of species with range overlap, particularly bearing in mind that the most common topology genome-wide may not represent the species tree. Although the identification of the species tree in these conditions remains challenging, systematic investigations of genome-wide phylogenetic variation in light of recombination rate may yield more accurate phylogenetic reconstructions and a better understanding of the factors underlying gene-tree heterogeneity.

Red- and Yellow-Fronted Tinkerbirds Maintain Phenotypic Integrity Despite Gene Flow

One important implication of our results is that RFT and YFT lineages can withstand very high levels of introgression across their whole ranges while maintaining their phenotypic integrity and genome-wide differentiation. Previous investigations of *extoni* and *pusillus* in Southern Africa suggest that variation in forecrown color and song rhythm might instigate assortative mating (Kirschel et al. 2020; Sebastianelli et al. 2024). In this hybrid zone, the phenotypic and genome-wide transitions are similarly sharp (Nwankwo et al. 2019; Sebastianelli et al. 2024), demonstrating that introgression does not compromise the phenotypic integrity of *pusillus* and *extoni*. The levels of gene-tree heterogeneity that we report across the whole species complex suggest that similar mechanisms play out in the other contact zones. The genetic architecture of forecrown color

and song rhythm appears relatively simple, with respectively 1 and 4 genes specifically identified so far (Kirschel et al. 2020; Sebastianelli et al. 2024). Thus, it is possible that reduced introgression at these loci combined with assortative mating contribute to maintaining phenotypic integrity in allopatric populations, whereas the genomic background is largely introgressed. Under this hypothesis, recombination would break the association between alleles associated with phenotypic traits and introgressing neutral variants (Barton and Bengtsson 1986; Martin and Jiggins 2017; Schumer et al. 2018), which is consistent with the genomic distribution of topology weights in our analysis, where many small windows that support RFT monophyly are interspersed across the genome. Particularly, 5 such windows overlap the gene CYP2J19 on chromosome 8, which has been identified as the ketolase that catalyzes the conversion of dietary yellow carotenoids to red ketocarotenoids and thus explains differences in forecrown coloration (Kirschel et al. 2020). This finding lends further support to the hypothesis that genes underlying phenotypic traits involved in reproductive isolation resist introgression, and are decoupled from introgressed variants by recombination. Other studies have reported sympatric or parapatric bird lineages where genomic divergence is concentrated in small genomic regions associated with phenotypic traits involved in assortative mating, whereas most of the genome flows freely (e.g., Toews et al. 2016; Campagna et al. 2017; Wang et al. 2020; Funk et al. 2021; Turbek et al. 2021). This, together with a growing body of evidence for widespread introgression across avian species (Ottenburghs et al. 2017), suggest that the maintenance of phenotypic integrity driven by a few genomic loci in the face of widespread gene flow may be a common phenomenon in birds. It should be noted, however, that the presence of loci with narrow clines throughout the genome, as well as the positive correlation between introgression and recombination rates, suggests a polygenic basis for reproductive isolation between YFT and RFT. Although loci coding for sexual signaling traits may play an important role in isolation, our results imply the existence of many small-effect barrier loci, potentially associated with local adaptation, and/or other phenotypic differences that could play a role in assortative mating, including in supercilium and wing-covert color (Kirschel et al. 2020). The lack of introgression between the yellow-fronted *chrysoconus* and *extoni* further supports the existence of other barriers to gene flow than forecrown coloration.

Although our results shine a new light on speciation mechanisms and the evolutionary history of red- and yellow-fronted tinkerbirds, several phenomena remain unexplained. Our topology weighting analyses revealed contrasting patterns in the autosomes and the Z chromosome. In the latter, the phylogenetic signal for a monophyletic *extoni* + *pusillus* was reduced, whereas several large clusters of windows supported monophyly in either the northern taxa *chrysoconus–xanthostictus* + *affinis–uropygialis* or the red-fronted taxa *affinis–uropygialis* + *pusillus*. This pattern suggests differential introgression on the Z chromosome across the different hybrid zones. Sex chromosomes play a major role in speciation, because their reduced recombination facilitates the emergence of reproductive incompatibilities (Irwin 2018). Because of that, sex chromosomes are generally considered to be less permeable to gene flow compared with autosomes (Muirhead and Presgraves 2016; Fraïsse and Sachdeva 2021), and have been used to identify the correct species relationships in the presence of introgression (Fontaine et al. 2015; Johnson et al. 2023; Jiang et al. 2024). However, cases of sex chromosome introgression have also been reported (Li et al. 2016; Jensen et al. 2024; Rancilhac et al. 2024). Further investigations will be required to clarify the role of sex chromosomes in tinkerbird speciation. Another puzzling aspect is the maintenance of ecological differences in the face of gene flow, as the four RFT and YFT lineages occupy distinct habitats and occur along ecological gradients (Kirschel et al. 2021; Sebastianelli et al. 2024). Nevertheless, introgression can be deleterious by acting against local adaptation (Kawecki and Ebert 2004). Similarly to phenotypic traits, the genetic architecture of local adaptation likely plays a key role in its maintenance in the face of gene flow (Tigano and Friesen 2016).

Conclusion

In this study, we combined phylogenomics and hybrid zone analyses in a group of closely related, parapatric bird species to understand the contribution of contemporary gene flow to gene-tree heterogeneity, and its relevance to understanding speciation mechanisms. Our results highlight that the genomes of red- and yellow-fronted tinkerbirds are mosaics of regions supporting different topologies as a result of introgression. Particularly, we demonstrate that contemporary gene flow through hybrid zones contributes to this pattern. Using genomic regions with the lowest recombination rate appears to be a relevant approach to identify the species relationships in the face of introgression.

Red- and yellow-fronted tinkerbirds appear to represent one more example where introgression results in the dominant phylogenetic signal being discordant with the species tree. This conclusion is especially important when investigating the evolution of forecrown coloration: although the genome-wide topology suggests parallel evolution of red and yellow forecrowns, our results support a single origin of red feather color. Thus, our study further demonstrates the relevance of phylogenetic analyses of whole-genome data to understand the evolution of phenotypic traits and, consequently, reproductive isolation.

Acknowledgments

We thank L. Hadjioannou, E.C. Nwankwo, M. Mamba, T.G. Hadjikyriakou, and K.G. Mortega for field-

work; A. Howland, S. Agostini, G. Vogt, the landowners of Kube Yini Private Game Reserve and of Seringveld, De Tweedespruit, and Cullinan Conservancies (especially E. Fourie and J. van Nieuwenhuizen, J. Visser, L. Klapwijk, J. Du Toit, and R. Olivier), S. Willows-Munro, C. Niesler, N. Baker and the late L. Baker, R. Mulwa, D. Pomeroy, and A. Monadjem for logistical support; and Louisiana State University Museum of Natural Science (D.L. Dittmann), the Zoological Museum of the University of Copenhagen (J. Bolding Kristensen), and the Center for Tropical Research at the University of California, Los Angeles (T.B. Smith) for providing samples. The Ethiopian Wildlife Conservation Authority, Uganda Wildlife Authority, Uganda National Council for Science and Technology, Kenya Wildlife Service, Kenya's National Council for Science and Technology, National Museums of Kenya, Tanzania Wildlife Research Institute (TAWIRI), Tanzania Commission for Science and Technology (COSTECH), Tanzania National Parks (TANAPA), Eswatini Big Game Parks, Ezemvelo KZN Wildlife, Mpumalanga Tourism and Parks Agency, Gauteng Department of Agriculture and Rural Development (GDARD), the Animal Research Ethics Committee of the University of KwaZulu-Natal (ref: AREC/00002381-82/2021), and the Cyprus Ministry of Agriculture, Rural Development and Environment Veterinary Services provided permits.

Author Contributions

L.R.: Conceptualization, Formal analysis, Methodology, Visualization, Writing—original draft preparation, Writing—review & editing; S.G.dS. and B.O.O.: Data curation, Writing—review & editing; S.M.L., M.S., T.A., and C.T.D.: Investigation, Resources, Writing—review & editing; M.M. and C.N.: Investigation, Writing—review & editing; A.B.: Methodology, Validation, Writing—review & editing; B.M.vH.: Conceptualization, Project administration, Resources, Methodology, Validation, Writing—review & editing; and A.N.G.K.: Conceptualization, Investigation, Funding acquisition, Project administration, Resources, Writing—review & editing.

Supplementary Material

Data available from the Dryad Digital Repository: https://doi.org/10.5061/dryad.0cfxpnwb3.

Conflict of Interest

None declared.

Funding

This work was supported by the European Regional Development Fund; the Research and Innovation Foundation Cyprus (projects EXCELLENCE/0421/0413 and EXCELLENCE/0421/0301); University of Cyprus [grant number 8037P-25023]; FP7 Marie Curie Reintegration [grant number 268316 to A.N.G.K.]; and A.G. Leventis Foundation scholarships [to S.G.dS., S.M.L., M.S., and M.M.].

Data Availability

The supplementary tables and figures, Appendix 1, and the data files necessary to reproduce the analyses and figures are available at (https://doi.org/10.5061/dryad.0cfxpnwb3). The scripts used to run the analyses and create the figures are available at https://github.com/rancilhac/Pogoniulus-phylogenomics-manuscript-data. WGS reads are available on the NCBI SRA (BioProjects PRJNA987636 and PRJNA1241442). ddRADseq reads are available at doi:10.5061/dryad.0cfxpnwb3 (https://doi.org/10.5061/dryad.0cfxpnwb3).

References

Alaei Kakhki N., Schweizer M., Lutgen D., Bowie R.C.K., Shirihai H., Suh A., Schielzeth H., Burri R. 2023. A phylogenomic assessment of processes underpinning convergent evolution in open-habitat chats. Mol. Biol. Evol. 40(1):msac278.

Alexander D.H., Novembre J., Lange K. 2009. Fast model-based estimation of ancestry in unrelated individuals. Genome Res. 19(9):1655–1664.

Barton N., Bengtsson B.O. 1986. The barrier to genetic exchange between hybridising populations. Heredity 57(3):357–376.

Barton N.H., Hewitt G.M. 1985. Analysis of hybrid zones. Annu. Rev. Ecol. Syst. 16(1):113–148.

Bravo G.A., Antonelli A., Bacon C.D., Bartoszek K., Blom M.P.K., Huynh S., Jones G., Knowles L.L., Lamichhaney S., Marcussen T., Morlon H., Nakhleh L.K., Oxelman B., Pfeil B., Schliep A., Wahlberg N., Werneck F.P., Wiedenhoeft J., Willows-Munro S., Edwards S.V. 2019. Embracing heterogeneity: coalescing the Tree of Life and the future of phylogenomics. PeerJ 7:e6399.

Brelsford A., Dufresnes C., Perrin N. 2016. High-density sex-specific linkage maps of a European tree frog (*Hyla arborea*) identify the sex chromosome without information on offspring sex. Heredity 116(2):177–181.

Broad Institute. 2019. Picard toolkit. http://broadinstitute.github.io/picard

Burbrink F.T., Gehara M. 2018. The biogeography of deep time phylogenetic reticulation. Syst. Biol. 67(5):743–755.

Caeiro-Dias G., Rocha S., Couto A., Pereira C., Brelsford A., Crochet P.-A., Pinho C. 2021. Nuclear phylogenies and genomics of a contact zone establish the species rank of *Podarcis lusitanicus* (Squamata, Lacertidae). Mol. Phylogenet. Evol. 164:107270.

Campagna L., Repenning M., Silveira L.F., Fontana C.S., Tubaro P.L., Lovette I.J. 2017. Repeated divergent selection on pigmentation genes in a rapid finch radiation. Sci. Adv. 3(5):e1602404.

Cruzan M.B., Thompson P.G., Diaz N.A., Hendrickson E.C., Gerloff K.R., Kline K.A., Machiorlete H.M., Persinger J.M. 2021. Weak coupling among barrier loci and waves of neutral and adaptive introgression across an expanding hybrid zone. Evolution 75(12):3098–3114.

Danecek P., Auton A., Abecasis G., Albers C.A., Banks E., DePristo M.A., Handsaker R.E., Lunter G., Marth G.T., Sherry S.T., McVean G., Durbin R., 1000 Genomes Project Analysis Group. 2011. The variant call format and VCFtools. Bioinformatics 27(15):2156–2158.

Danecek P., Bonfield J.K., Liddle J., Marshall J., Ohan V., Pollard M.O., Whitwham A., Keane T., McCarthy S.A., Davies R.M., Li H. 2021. Twelve years of SAMtools and BCFtools. Gigascience 10(2):giab008.
Degnan J.H., Rosenberg N.A. 2009. Gene tree discordance, phylogenetic inference and the multispecies coalescent. Trends Ecol. Evol. 24(6):332–340.
del Hoyo J., Hanna M., Sargatal J., Christie D., Kirwan G. 2020. Handbook of the birds of the world alive. Barcelona: Lynx Edicions.
Derryberry E.P., Derryberry G.E., Maley J.M., Brumfield R.T. 2014. HZAR: hybrid zone analysis using an R software package. Mol. Ecol. Resour. 14(3):652–663.
Dufresnes C., Brelsford A., Jeffries D.L., Mazepa G., Suchan T., Canestrelli D., Nicieza A., Fumagalli L., Dubey S., Martínez-Solano I., Litvinchuk S.N., Vences M., Perrin N., Crochet P.-A. 2021. Mass of genes rather than master genes underlie the genomic architecture of amphibian speciation. Proc. Natl. Acad. Sci. USA 118(36):e2103963118.
Duranton M., Pool J.E. 2022. Interactions between natural selection and recombination shape the genomic landscape of introgression. Mol. Biol. Evol. 39(7):msac122.
Edelman N.B., Mallet J. 2021. Prevalence and adaptive impact of introgression. Annu. Rev. Genet. 55(1):265–283.
Feng S., Bai M., Rivas-González I., Li C., Liu S., Tong Y., Yang H., Chen G., Xie D., Sears K.E., Franco L.M., Gaitan-Espitia J.D., Nespolo R.F., Johnson W.E., Yang H., Brandies P.A., Hogg C.J., Belov K., Renfree M.B., Helgen K.M., Boomsma J.J., Schierup M.H., Zhang G. 2022. Incomplete lineage sorting and phenotypic evolution in marsupials. Cell 185(10):1646–1660. e18.
Feng X., Merilä J., Löytynoja A. 2024. Secondary contact, introgressive hybridization, and genome stabilization in sticklebacks. Mol. Biol. Evol. 41(2):msae031.
Ferreira M.S., Jones M.R., Callahan C.M., Farelo L., Tolesa Z., Suchentrunk F., Boursot P., Mills L.S., Alves P.C., Good J.M., Melo-Ferreira J. 2021. The legacy of recurrent introgression during the radiation of hares. Syst. Biol. 70(3):593–607.
Foley N.M., Harris A.J., Bredemeyer K.R., Ruedi M., Puechmaille S.J., Teeling E.C., Criscitiello M.F., Murphy W.J. 2024. Karyotypic stasis and swarming influenced the evolution of viral tolerance in a species-rich bat radiation. Cell Genom. 4(2):100482.
Fontaine M.C., Pease J.B., Steele A., Waterhouse R.M., Neafsey D.E., Sharakhov I.V., Jiang X., Hall A.B., Catteruccia F., Kakani E., Mitchell S.N., Wu Y.-C., Smith H.A., Love R.R., Lawniczak M.K., Slotman M.A., Emrich S.J., Hahn M.W., Besansky N.J. 2015. Extensive introgression in a malaria vector species complex revealed by phylogenomics. Science 347(6217):1258524.
Fraïsse C., Sachdeva H. 2021. The rates of introgression and barriers to genetic exchange between hybridizing species: sex chromosomes vs autosomes. Genetics 217(2):iyaa025.
Funk E.R., Mason N.A., Pálsson S., Albrecht T., Johnson J.A., Taylor S.A. 2021. A supergene underlies linked variation in color and morphology in a Holarctic songbird. Nat. Commun. 12(1):6833.
Grossen C., Seneviratne S.S., Croll D., Irwin D.E. 2016. Strong reproductive isolation and narrow genomic tracts of differentiation among three woodpecker species in secondary contact. Mol. Ecol. 25(17):4247–4266.
Hennelly L.M., Habib B., Modi S., Rueness E.K., Gaubert P., Sacks B.N. 2021. Ancient divergence of Indian and Tibetan wolves revealed by recombination-aware phylogenomics. Mol. Ecol. 30(24): 6687–6700.
Hibbins M.S., Hahn M.W. 2022. Phylogenomic approaches to detecting and characterizing introgression. Genetics 220(2):iyab173.
Irwin D.E. 2018. Sex chromosomes and speciation in birds and other ZW systems. Mol. Ecol. 27(19):3831–3851.
Jeffroy O., Brinkmann H., Delsuc F., Philippe H. 2006. Phylogenomics: the beginning of incongruence? Trends Genet. 22(4):225–231.
Jensen A., Horton E.R., Amboko J., Parke S.A., Hart J.A., Tosi A.J., Guschanski K., Detwiler K.M. 2024. Y chromosome introgression between deeply divergent primate species. Nat. Commun. 15(1):1–15.
Jiang Z., Zang W., Ericson P.G.P., Song G., Wu S., Feng S., Drovetski S.V., Liu G., Zhang D., Saitoh T., Alström P., Edwards S.V., Lei F., Qu Y. 2024. Gene flow and an anomaly zone complicate phylogenomic inference in a rapidly radiated avian family (Prunellidae). BMC Biol. 22(1):49.
Johnson J.A., Novak B., Athrey G., Sharo A.G., Chase T., Toepfer J. 2023. Phylogenomics of the extinct Heath Hen provides support for sex-biased introgression among extant prairie grouse. Mol. Phylogenet. Evol. 189:107927.
Jombart T., Dray S. 2010. Adephylo: exploratory analyses for the phylogenetic comparative method. Bioinformatics 26(15):1–21.
Jukes T.H., Cantor C.R. 1969. Evolution of protein molecules. Mamm. Protein Metab. 3:21–132.
Kawecki T.J., Ebert D. 2004. Conceptual issues in local adaptation. Ecol. Lett. 7(12):1225–1241.
Khan M., Joshi M., Espeland M., Huemer P., Lopez-Vaamonde C., Mutanen M. 2024. Patterns of speciation in a parapatric pair of *Saturnia* moths as revealed by target capture. Mol. Ecol. 33(1):e17194.
Kirschel A.N.G., Moysi M., Lukhele S.M., Sebastianelli M., Asfaw T., Hadjioannou L., Mortega K.G., Monadjem A., Moyle R.G. 2021. Taxonomic revision of the red-fronted tinkerbird *Pogoniulus pusillus* (Dumont, 1816) based on molecular and phenotypic analyses. Bull. Br. Ornithol. Club 141(4):428–442.
Kirschel A.N.G., Nwankwo E.C., Pierce D.K., Lukhele S.M., Moysi M., Ogolowa B.O., Hayes S.C., Monadjem A., Brelsford A. 2020. CYP2J19 mediates carotenoid colour introgression across a natural avian hybrid zone. Mol. Ecol. 29(24):4970–4984.
Kirschel A.N.G., Sebastianelli M. 2022. A reassessment of the East African ranges of two subspecies of yellow-fronted tinkerbird *Pogoniulus chrysoconus* based on a comparison of plumage, biometrics and song. Scopus: J. East Afr. Ornithol. 42:1–9.
Li G., Davis B.W., Eizirik E., Murphy W.J. 2016. Phylogenomic evidence for ancient hybridization in the genomes of living cats (Felidae). Genome Res. 26(1):1–11.
Li G., Figueiró H.V., Eizirik E., Murphy W.J. 2019. Recombination-aware phylogenomics reveals the structured genomic landscape of hybridizing cat species. Mol. Biol. Evol. 36(10):2111–2126.
Li H., Durbin R. 2009. Fast and accurate short read alignment with Burrows–Wheeler transform. Bioinformatics 25(14):1754–1760.
Mai U., Mirarab S. 2018. TreeShrink: fast and accurate detection of outlier long branches in collections of phylogenetic trees. BMC Genomics 19(S5):23–40.
Malinsky M., Challis R.J., Tyers A.M., Schiffels S., Terai Y., Ngatunga B.P., Miska E.A., Durbin R., Genner M.J., Turner G.F. 2015. Genomic islands of speciation separate cichlid ecomorphs in an East African crater lake. Science 350(6267):1493–1498.
Malinsky M., Matschiner M., Svardal H. 2021. Dsuite—fast D-statistics and related admixture evidence from VCF files. Mol. Ecol. Resour. 21(2):584–595.
Mallet J., Besansky N., Hahn M.W. 2016. How reticulated are species? Bioessays 38(2):140–149.
Martin M. 2011. Cutadapt removes adapter sequences from high-throughput sequencing reads. EMBnet. 17 (1):10–12.
Martin S.H., Davey J.W., Salazar C., Jiggins C.D. 2019. Recombination rate variation shapes barriers to introgression across butterfly genomes. PLoS Biol. 17(2):e2006288.
Martin S.H., Jiggins C.D. 2017. Interpreting the genomic landscape of introgression. Curr. Opin. Genet. Dev. 47:69–74.
Martin S.H., Van Belleghem S.M. 2017. Exploring evolutionary relationships across the genome using topology weighting. Genetics 206(1):429–438.
McKenna A., Hanna M., Banks E., Sivachenko A., Cibulskis K., Kernytsky A., Garimella K., Altshuler D., Gabriel S., Daly M., DePristo M.A. 2010. The genome analysis toolkit: a mapreduce framework for analyzing next-generation DNA sequencing data. Genome Res. 20(9):1297–1303.
Meier J.I., McGee M.D., Marques D.A., Mwaiko S., Kishe M., Wandera S., Neumann D., Mrosso H., Chapman L.J., Chapman C.A., Kaufman L., Taabu-Munyaho A., Wagner C.E., Bruggmann R., Excoffier L., Seehausen O. 2023. Cycles of fusion and fission enabled rapid parallel adaptive radiations in African cichlids. Science 381(6665):eade2833.

Mirarab S., Reaz R., Bayzid Md.S., Zimmermann T., Swenson M.S., Warnow T. 2014. ASTRAL: genome-scale coalescent-based species tree estimation. Bioinformatics 30(17):i541–i548.
Muirhead C.A., Presgraves D.C. 2016. Hybrid incompatibilities, local adaptation, and the genomic distribution of natural introgression between species. Am. Nat. 187(2):249–261.
Musher L.J., Del-Rio G., Marcondes R.S., Brumfield R.T., Bravo G.A., Thom G. 2024. Geogenomic predictors of genetree heterogeneity explain phylogeographic and introgression history: a case study in an Amazonian bird (*Thamnophilus aethiops*). Syst. Biol. 73(1): 36–52.
Nwankwo E.C., Mortega K.G., Karageorgos A., Ogolowa B.O., Papagregoriou G., Grether G.F., Monadjem A., Kirschel A.N.G. 2019. Rampant introgressive hybridization in *Pogoniulus* tinkerbirds (Piciformes: Lybiidae) despite millions of years of divergence. Biol. J. Linn. Soc. 127(1):125–142.
Ottenburghs J., Kraus R.H., van Hooft P., van Wieren S.E., Ydenberg R.C., Prins H.H. 2017. Avian introgression in the genomic era. Avian Research. 8:1–11.
Parchman T.L., Gompert Z., Mudge J., Schilkey F.D., Benkman C.W., Buerkle C.A. 2012. Genome-wide association genetics of an adaptive trait in lodgepole pine. Mol. Ecol. 21(12):2991–3005.
Payseur B.A. 2010. Using differential introgression in hybrid zones to identify genomic regions involved in speciation. Mol. Ecol. Resour. 10(5):806–820.
Pease J.B., Haak D.C., Hahn M.W., Moyle L.C. 2016. Phylogenomics reveals three sources of adaptive variation during a rapid radiation. PLoS Biol. 14(2):e1002379.
Pease J.B., Hahn M.W. 2013. More accurate phylogenies inferred from low-recombination regions in the presence of incomplete lineage sorting. Evolution 67(8):2376–2384.
Peterson B.K., Weber J.N., Kay E.H., Fisher H.S., Hoekstra H.E. 2012. Double digest RADseq: an inexpensive method for *de novo* SNP discovery and genotyping in model and non-model species. PLoS One 7(5):e37135.
Price T. 2008. Speciation in birds. Greenwood Village (CO): Roberts & Company Publishers.
Pulido-Santacruz P., Aleixo A., Weir J.T. 2018. Morphologically cryptic Amazonian bird species pairs exhibit strong postzygotic reproductive isolation. Proc. Biol. Sci. 285(1874):20172081.
Pulido-Santacruz P., Aleixo A., Weir J.T. 2020. Genomic data reveal a protracted window of introgression during the diversification of a neotropical woodcreeper radiation. Evolution 74(5): 842–858.
Racimo F., Sankararaman S., Nielsen R., Huerta-Sánchez E. 2015. Evidence for archaic adaptive introgression in humans. Nat. Rev. Genet. 16(6):359–371.
Rancilhac L., Enbody E.D., Harris R., Saitoh T., Irestedt M., Liu Y., Lei F., Andersson L., Alström P. 2024. Introgression underlies phylogenetic uncertainty but not parallel plumage evolution in a recent songbird radiation. Syst. Biol. 73(1):12–25.
Rancilhac L., Irisarri I., Angelini C., Arntzen J.W., Babik W., Bossuyt F., Künzel S., Lüddecke T., Pasmans F., Sanchez E., Weisrock D., Veith M., Wielstra B., Steinfartz S., Hofreiter M., Philippe H., Vences M. 2021. Phylotranscriptomic evidence for pervasive ancient hybridization among Old World salamanders. Mol. Phylogenet. Evol. 155:106967.
Rochette N.C., Rivera-Colón A.G., Catchen J.M. 2019. Stacks 2: analytical methods for paired-end sequencing improve RADseq-based population genomics. Mol. Ecol. 28(21):4737–4754.
Sarver B.A.J., Herrera N.D., Sneddon D., Hunter S.S., Settles M.L., Kronenberg Z., Demboski J.R., Good J.M., Sullivan J. 2021. Diversification, introgression, and rampant cytonuclear discordance in Rocky Mountains chipmunks (Sciuridae: *Tamias*). Syst. Biol. 70(5):908–921.
Schumer M., Xu C., Powell D.L., Durvasula A., Skov L., Holland C., Blazier J.C., Sankararaman S., Andolfatto P., Rosenthal G.G., Przeworski M. 2018. Natural selection interacts with recombination to shape the evolution of hybrid genomes. Science 360(6389): 656–660.
Scornavacca C., Galtier N. 2017. Incomplete lineage sorting in mammalian phylogenomics. Syst. Biol. 66:112–120.
Sebastianelli M., Lukhele S.M., Nwankwo E.C., Hadjioannou L., Kirschel A.N.G. 2022. Continent-wide patterns of song variation predicted by classical rules of biogeography. Eco Lett. 5:2448–2462.
Sebastianelli M., Lukhele S.M., Secomandi S., de Souza S.G., Haase B., Moysi M., Nikiforou C., Hutfluss A., Mountcastle J., Balacco J., Pelan S., Chow W., Fedrigo O., Downs C.T., Monadjem A., Dingemanse N.J., Jarvis E.D., Brelsford A., vonHoldt B.M., Kirschel A.N.G. 2024. A genomic basis of vocal rhythm in birds. Nat. Commun. 15(1): 3095.
Singhal S., Derryberry G.E., Bravo G.A., Derryberry E.P., Brumfield R.T., Harvey M.G. 2021. The dynamics of introgression across an avian radiation. Evol. Lett. 5(6):568–581.
Smith J., Kronforst M.R. 2013. Do Heliconius butterfly species exchange mimicry alleles? Biol. Lett. 9(4):20130503.
Stankowski S., Zagrodzka Z.B., Garlovsky M.D., Pal A., Shipilina D., Castillo D.G., Lifchitz H., Le Moan A., Leder E., Reeve J., Johannesson K., Westram A.M., Butlin R.K. 2024. The genetic basis of a recent transition to live-bearing in marine snails. Science 383(6678):114–119.
Suvorov A., Scornavacca C., Fujimoto M.S., Bodily P., Clement M., Crandall K.A., Whiting M.F., Schrider D.R., Bybee S.M. 2022. Deep ancestral introgression shapes evolutionary history of dragonflies and damselflies. Syst. Biol. 71(3):526–546.
Svardal H., Quah F.X., Malinsky M., Ngatunga B.P., Miska E.A., Salzburger W., Genner M.J., Turner G.F., Durbin R. 2020. Ancestral hybridization facilitated species diversification in the Lake Malawi cichlid fish adaptive radiation. Mol. Biol. Evol. 37(4): 1100–1113.
Szymura J.M., Barton N.H. 1986. Genetic analysis of a hybrid zone between the fire-bellied toads, *Bombina bombina* and *B. variagata*, near Cracow in Southern Poland. Evolution 40:1141–1159.
Thom G., Amaral F.R.D., Hickerson M.J., Aleixo A., Araujo-Silva L.E., Ribas C.C., Choueri E., Miyaki C.Y. 2018. Phenotypic and genetic structure support gene flow generating gene tree discordances in an Amazonian floodplain endemic species. Syst. Biol. 67(4): 700–718.
Thom G., Moreira L.R., Batista R., Gehara M., Aleixo A., Smith B.T. 2024. Genomic architecture predicts tree topology, population structuring, and demographic history in Amazonian birds. Genome Biol. Evol. 16(1):evae002.
Tigano A., Friesen V.L. 2016. Genomics of local adaptation with gene flow. Mol. Ecol. 25(10):2144–2164.
Toews D.P., Taylor S.A., Vallender R., Brelsford A., Butcher B.G., Messer P.W., Lovette I.J. 2016. Plumage genes and little else distinguish the genomes of hybridizing warblers. Curr. Biol. 26(17):2313–2318.
Turbek S.P., Browne M., Di Giacomo A.S., Kopuchian C., Hochachka W.M., Estalles C., Lijtmaer D.A., Tubaro P.L., Silveira L.F., Lovette I.J., Safran R.J., Taylor S.A., Campagna L. 2021. Rapid speciation via the evolution of pre-mating isolation in the Iberá seedeater. Science. 371(6536):eabc0256.
Vanderpool D., Minh B.Q., Lanfear R., Hughes D., Murali S., Harris R.A., Raveendran M., Muzny D.M., Hibbins M.S., Williamson R.J., Gibbs R.A., Worley K.C., Rogers J., Hahn M.W. 2020. Primate phylogenomics uncovers multiple rapid radiations and ancient interspecific introgression. PLoS Biol. 18(12): e3000954.
Wang S., Rohwer S., de Zwaan D.R., Toews D.P., Lovette I.J., Mackenzie J., Irwin D. 2020. Selection on a small genomic region underpins differentiation in multiple color traits between two warbler species. Evol. Lett., 4(6):502–515.
Zhang D., Rheindt F.E., She H., Cheng Y., Song G., Jia C., Qu Y., Alström P., Lei F. 2021. Most genomic loci misrepresent the phylogeny of an avian radiation because of ancient gene flow. Syst. Biol. 70:961–975.

Syst. Biol. 74(6):935–951, 2025

https://doi.org/10.1093/sysbio/syaf033
Advance Access publication May 13, 2025